

Local properties and Density of States in the two-dimensional p-d Model

V. Fiorentino, F. Mancini, and E. Žgžinas*

*Dipartimento di Scienze Fisiche "E.R. Caianiello" - Unità INFM di Salerno,
Università degli Studi di Salerno, 84081 Baronissi (SA), Italy*

A. F. Barabanov

Institute for High Pressure Physics, 142098 Troitsk, Moscow Region, Russia

(November 14, 2018)

The p-d model which well describes the CuO_2 planes of the high- T_c superconductors is studied by means of the Composite Operator Method (COM). The relevant quasi-particle excitations are represented by composite operators. As a result of taking into account spin excitations we find a p -like band near the Fermi level. The dispersion of this band gives a Fermi surface which is in good agreement with the experimental measurements. Due to the strong mixing of the relevant excitations, the spectral weight of this band is reduced and gives a large Fermi surface in the moderately doped region. The dependence of the calculated physical quantities on model parameters, temperature and doping, is in a very good agreement with the available Quantum Monte Carlo results.

71.18.+y, 74.25.Bt, 74.25.Jb, 75.20.Hr

I. INTRODUCTION

Many unexplained exotic features of transition metal oxides containing CuO_2 planes [1,2] have inspired the developing of various theoretical methods to solve, at least approximately, the models which describe such compounds.

In the last years, a big effort has been devoted to explain experimental results in terms of Hubbard-like or t-J models and many interesting results have been successfully achieved. The Hubbard model was suggested [3,4] as low energy derivative of the Emery (or p-d) three band model [5]. The Emery model takes into account the crystalline structure of CuO_2 planes and initially retains the orbitals of p and d electrons at oxygen and copper sites, the d orbital giving the strong Coulomb repulsion when occupied by two electrons. Due to the more detailed structure of the p-d model, one can expect that its solutions can give us a more rich physical picture of cuprates and can explain a wider range of experimental results than solutions of Hubbard-like or t-J models.

It is believed that the strong correlation of electrons in the copper d orbitals leads both to the insulating antiferromagnetic state at low density of doping carriers and to superconductivity at higher doping. The doping dependence of the electronic state is not rigid band-like. This suggests that the doped hole changes the state of nearby localized copper d electron and reduces the energy of the system if compared to the case of rigid band doping.

A detailed mechanism of binding d electron to the doped hole was proposed by Zhang and Rice [4]. As a result of binding, a local singlet forms and it can move through the lattice. Further theoretical investigations of the band dispersion of such singlet in CuO_2 planes gave a successful description [6,7] of ARPES results [8–11].

However, to recover the doping and temperature de-

pendence of micro- and macro-scopic observables, one needs to study not only such singlet excitations, although their energy lies near the Fermi level, but also the wider basis of excitations which are possible in the plane.

Recently, a technique called the Composite Operator Method (COM) has been proposed [12–14] to describe the local and itinerant properties of strongly correlated systems. A physical model is usually described in terms of elementary particles and some interaction. However, at level of observation the identity of the original particles is lost; the macroscopic behavior of the system is described in terms of new excitation modes. When the interaction is strong the properties of these excitations will be very different from those of the original particles and hardly obtainable by a perturbation scheme. By following this scheme, in the COM a set of field operators is taken as the basis in which the theory is developed. These fields are chosen in order to describe the experimentally observed properties and are called composite fields since they are constructed from the initial set of particles. The properties of these composite fields are dynamically determined by the interaction and by the boundary conditions and must be self consistently calculated. In this process a special attention is put to preserve the symmetry properties of the model [15,16]. Particularly, the conservation of the Pauli principles plays a fundamental role. As discussed in Ref. [15], although the method has many points in common with the projection method [17], the method of equation of motion [18] and the spectral density approach [19], remarkable differences arise according to the different schemes of self consistency. The method has been applied to the study of several models, like Hubbard [13–15,20], t-J [21] and p-d [12,22,23] models.

The insufficiency of studying only those electronic states with energy close to the Fermi level was shown

in Ref. [12]. The reduced p-d model, where the transitions to the lower Hubbard level are neglected, was studied within a four-pole expansion for the Green's function. The fields were taken as the bare p electron, the upper Hubbard field, the p electron field with spin-flips at copper sites and the p electron operator with p-d charge-transfer.

In this work we investigate the full p-d model with a four-component field constituted by p electrons, lower and upper Hubbard operators for d electrons and a fourth field which describes p electrons dressed by spin fluctuations of d electrons. Some preliminary results were given in Ref. [24], where in particular we showed the necessity of introducing the fourth field. The model treated in terms of only the first three fields gives results not in agreement with the numerical simulation data and that do not give a satisfactory description of the experimental situation.

In Sec. II we present the p-d Hamiltonian and introduce the excitation modes represented in terms of composite field operators. The Green's function for these operators is calculated in the four-pole approximation and depends on a set of parameters expressed as equal-time correlation functions. The study of these parameters is given in Sec. III, where by using the symmetry imposed by the Pauli principle we derive a set of equations which allow us to obtain a complete self-consistent solution.

The developing of numerical methods, as Quantum Monte Carlo (QMC) and exact diagonalization [25], offers a new challenge to theoreticians. Before looking at the physical implication of the model one should be confident with the solution by calculating some quantities and comparing them with the data of numerical simulations. According to this, in Sec. IV A we make a detailed comparison of our results with the available data obtained by QMC studies. The comparison shows a very good agreement signaling us that the choice of the composite field and the self-consistent procedure adopted are able to give a reasonable solution of the model. We then proceed in sections IV B and IV C to analyze some physical properties. Section V is devoted to concluding remarks. Details of calculations are given in Appendix.

II. THE P-D MODEL WITHIN THE FRAMEWORK OF COMPOSITE OPERATOR METHOD

In this section we consider the p-d model and we present the relevant features of the Composite Operator Method. Starting from the tight-binding model [5] composed of d electrons in $3d_{x^2-y^2}$ copper orbitals and p electrons in $2p_{x,y}$ oxygen orbitals in a CuO_2 plane and considering only bonding p electrons [26], we keep the terms describing the strong intra-atomic Coulomb repulsion at Cu sites and the p and d electrons hopping.

Therefore, the original Hamiltonian of the p-d model can be written as

$$H = \sum_i \left[(\varepsilon_d - \mu) d^\dagger(i) d(i) + (\varepsilon_p - \mu) p^\dagger(i) p(i) + U n_\uparrow(i) n_\downarrow(i) + 2t \left(p^{\gamma\dagger}(i) d(i) + d^\dagger(i) p^\gamma(i) \right) \right] \quad (2.1)$$

where in the spinor notation $p^\dagger_\sigma(i)$ and $d^\dagger_\sigma(i)$ create a p electron and a d electron on site $i \equiv (\mathbf{R}_i, t_i)$ with spin projection $\sigma \in \{\uparrow, \downarrow\}$, respectively. μ is the chemical potential, the U term describes the Coulomb repulsion at Cu sites, $n_\sigma(i) = d^\dagger_\sigma(i) d_\sigma(i)$ is the charge density operator of d electrons with spin σ . The t term describes the p-d hopping and $p^\gamma(i)$ is defined by

$$p^\gamma(i) = \sum_j \gamma_{ij} p(j). \quad (2.2)$$

Here γ_{ij} is given by

$$\gamma_{ij} = \frac{a^2}{(2\pi)^2} \int_{\Omega_B} d^2\mathbf{k} e^{i\mathbf{k}\cdot(\mathbf{R}_i - \mathbf{R}_j)} \gamma(\mathbf{k}), \quad (2.3)$$

where Ω_B is the volume of the first Brillouin zone, $\gamma(\mathbf{k}) = \sqrt{1 - \alpha(\mathbf{k})}$ and where for a two-dimensional quadratic lattice with lattice constant a

$$\alpha(\mathbf{k}) = \frac{1}{2} [\cos(k_x a) + \cos(k_y a)]. \quad (2.4)$$

Due to the strong correlation among electrons we introduce the composite field

$$\Psi(i) \equiv \begin{pmatrix} p(i) \\ \xi(i) \\ \eta(i) \\ p_s(i) \end{pmatrix}, \quad (2.5)$$

where

$$\xi(i) = [1 - n(i)] d(i), \quad \eta(i) = n(i) d(i) \quad (2.6)$$

are the Hubbard operators which describe the basic excitations $n(i) = 0 \leftrightarrow n(i) = 1$ and $n(i) = 1 \leftrightarrow n(i) = 2$ on the lattice site i , respectively. The fourth field is chosen as

$$p_s(i) = \sigma_k n_k(i) p^\gamma(i) - \frac{3c}{I_{22}} \xi(i) - \frac{3b}{I_{33}} \eta(i). \quad (2.7)$$

The parameters b and c and the quantities I_{22} and I_{33} are given in Appendix.

We have introduced the charge- ($\mu = 0$) and spin- ($\mu = 1, 2, 3$) density operator of d electrons

$$n_\mu(i) = d^\dagger(i) \sigma_\mu d(i), \quad (2.8)$$

and we are using the following notation

$$\sigma_\mu \equiv (1, \vec{\sigma}), \quad \sigma^\mu \equiv (-1, \vec{\sigma}) \quad (2.9)$$

with σ_k ($k = 1, 2, 3$) being the Pauli matrices.

The choice of the composite field (2.5) is dictated by the following considerations. The strong intra-atomic Coulomb interaction at Cu sites induces a splitting of the d band into the lower and the upper Hubbard subbands. The large covalence between oxygen and copper electrons leads to a large fluctuation of the energy of p electrons at O sites. The field p_s , describing p -electronic excitations accompanied by the nearest neighbor d -electron spin fluctuations, represents electronic excitations associated with the Cu-O bonds.

The Heisenberg equations of motion for the composite field $\Psi(i)$ are

$$i \frac{\partial}{\partial t} \Psi(i) = [\Psi(i), H]$$

$$= \begin{pmatrix} (\varepsilon_p - \mu)p(i) + 2t[\xi^\gamma(i) + \eta^\gamma(i)] \\ (\varepsilon_d - \mu)\xi(i) + 2tp^\gamma(i) + 2t\pi(i) \\ (\varepsilon_d - \mu + U)\eta(i) - 2t\pi(i) \\ (\varepsilon_p - \mu)p_s(i) + \varepsilon_{pp}p^\gamma(i) + \varepsilon_{p\xi}\xi(i) \\ + \varepsilon_{p\eta}\eta(i) + t_p\pi(i) + 2t\kappa_s(i) \end{pmatrix}, \quad (2.10)$$

where the coupling constants ε_{pp} , $\varepsilon_{p\xi}$, $\varepsilon_{p\eta}$, t_p and the higher order operators $\pi(i)$ and $\kappa_s(i)$ are defined by the following relations:

$$\varepsilon_{pp} = -\frac{6tc}{I_{22}}, \quad \varepsilon_{p\xi} = \frac{3c(\varepsilon_p - \varepsilon_d)}{I_{22}}, \quad (2.11)$$

$$\varepsilon_{p\eta} = \frac{3b(\varepsilon_p - \varepsilon_\eta)}{I_{33}}, \quad t_p = 6t \left(\frac{b}{I_{33}} - \frac{c}{I_{22}} \right), \quad (2.12)$$

$$\pi(i) = \frac{1}{2}\sigma^\mu n_\mu(i)p^\gamma(i) + \xi(i)p^{\gamma^\dagger}(i)\eta(i), \quad (2.13)$$

$$\kappa_s(i) = \sigma_k d^\dagger(i)\sigma_k p^\gamma(i)p^\gamma(i) - \sigma_k p^{\gamma^\dagger}(i)\sigma_k d(i)p^\gamma(i) + \sigma_k n_k(i)d^{\gamma^2}(i). \quad (2.14)$$

Let us introduce the thermal retarded Green's function

$$S(i, j) \equiv \langle R [\Psi(i)\Psi^\dagger(j)] \rangle, \quad (2.15)$$

where R is the usual retarded operator and the bracket $\langle \dots \rangle$ denotes the thermal average on the grand canonical ensemble. Use of equation of motion (2.10) will generate an infinite hierarchy of coupled equations and we need to introduce some approximation. To this purpose, let us split the Heisenberg equation (2.10) into a linear and nonlinear part

$$i \frac{\partial}{\partial t} \Psi(i) = \sum_j \varepsilon(i, j)\Psi(j) + \delta J(i), \quad (2.16)$$

where the equal-time correlation matrix $\varepsilon(i, j)$, the so-called energy matrix, is fixed by the requirement that the nonlinear term $\delta J(i)$ is orthogonal to the fundamental basis (2.5):

$$\langle \{\delta J(i), \Psi^\dagger(j)\}_{E.T.} \rangle = 0. \quad (2.17)$$

In the framework of the pole approximation we neglect the nonlinear term $\delta J(i)$ in the equation of motion. Then, for a translational invariant system the Fourier transform $S(\mathbf{k}, \omega)$ of the retarded propagator has the following expression

$$S(\mathbf{k}, \omega) = \frac{1}{\omega - \varepsilon(\mathbf{k})} I(\mathbf{k}), \quad (2.18)$$

where $\varepsilon(\mathbf{k})$, the Fourier transform of the energy matrix, can be expressed as

$$\varepsilon(\mathbf{k}) = m(\mathbf{k})I^{-1}(\mathbf{k}). \quad (2.19)$$

In order to simplify the notation we introduced the so-called normalization matrix $I(\mathbf{k})$ and the so-called mass matrix $m(\mathbf{k})$

$$I(\mathbf{k}) \equiv F.T. \langle \{\Psi(i), \Psi^\dagger(j)\}_{E.T.} \rangle, \quad (2.20)$$

$$m(\mathbf{k}) \equiv F.T. \left\langle \left\{ i \frac{\partial}{\partial t} \Psi(i), \Psi^\dagger(j) \right\}_{E.T.} \right\rangle, \quad (2.21)$$

where the symbol $F.T.$ denotes the Fourier transform. Straightforward calculations give the expressions of these matrices. The results for a paramagnetic state are given in Appendix. The Green's function (2.18) can be put in the spectral form

$$S(\mathbf{k}, \omega) = \sum_{n=1}^4 \frac{\sigma^{(n)}(\mathbf{k})}{\omega - E_n(\mathbf{k}) + i\delta}. \quad (2.22)$$

The energy-spectra $E_n(\mathbf{k})$ are the eigenvalues of the $\varepsilon(\mathbf{k})$ matrix and the spectral functions $\sigma^{(n)}(\mathbf{k})$ are given by

$$\sigma_{ab}^{(n)}(\mathbf{k}) = \sum_{c=1}^4 \Lambda_{an}(\mathbf{k}) \Lambda_{nc}^{-1}(\mathbf{k}) I_{cb}(\mathbf{k}), \quad (2.23)$$

where $a, b = 1, \dots, 4$ and where the columns of the $\Lambda(\mathbf{k})$ matrix are the eigenvectors of the $\varepsilon(\mathbf{k})$ matrix.

Summarizing, in our scheme of calculations firstly we choose a fundamental basis of Heisenberg composite operators. The propagator for this basic field is evaluated in a pole approximation, where the incoherent part is neglected. The main ingredient of the calculation is the energy matrix. The knowledge of this function will allow us to calculate the excitations of the system and the spectral functions. The entire process requires a self-consistent procedure which will be discussed in the next Section.

III. CORRELATION FUNCTIONS AND SELF-CONSISTENT EQUATIONS

In this section we introduce the correlation functions and give the expressions of the self-consistent equations needed to calculate the fermionic propagator.

As shown in Appendix, the Green's function depends on a set of parameters expressed as static correlation functions of composite operators. Some of these operators belong to the basic set (2.5) and their expectation values are directly connected to matrix elements of the Green's function. Other operators are composite fields of higher order, out of the basis (2.5), and their correlation functions must be evaluated by other means. This aspect is a general property of the Green's function method [27]. These functions refer to a specific choice of the Hilbert space and one must specify the proper representation. In particular, the states must be constructed in such a way that the relations imposed by the Pauli principle must be satisfied at level of expectation values.

Let us introduce the correlation function

$$C(i, j) = \langle \Psi(i) \Psi^\dagger(j) \rangle. \quad (3.1)$$

By means of the spectral theorem and by recalling Eq. (2.22), this function has the expression

$$C(i, j) = \frac{a^2}{2(2\pi)^2} \sum_{n=1}^4 \int_{\Omega_B} d^2\mathbf{k} e^{i\mathbf{k}\cdot(\mathbf{R}_i - \mathbf{R}_j) - iE_n(\mathbf{k})(t_i - t_j)} \times [1 + T_n(\mathbf{k})] \sigma^{(n)}(\mathbf{k}), \quad (3.2)$$

where

$$T_n(\mathbf{k}) = \tanh\left(\frac{E_n(\mathbf{k})}{2k_B T}\right). \quad (3.3)$$

The parameters directly connected to the Green's function are: n_d , a_s , b , b_s , c , D . By means of the definitions given in Appendix, we have the self-consistent equations

$$n_d = 2(1 - C_{22} - C_{33}), \quad (3.4)$$

$$a_s = C_{14}^\gamma + \frac{3c}{I_{22}} C_{12}^\gamma + \frac{3b}{I_{33}} C_{13}^\gamma, \quad (3.5)$$

$$b = C_{13}^\gamma, \quad (3.6)$$

$$b_s = C_{24}^\alpha + C_{34}^\alpha + \frac{3c}{I_{22}} [C_{22}^\alpha + C_{23}^\alpha] + \frac{3b}{I_{33}} [C_{23}^\alpha + C_{33}^\alpha], \quad (3.7)$$

$$c = C_{12}^\gamma, \quad (3.8)$$

$$D = I_{33} - C_{33}. \quad (3.9)$$

We are using the following notation

$$C_{\mu\nu} = C_{\mu\nu}(i, i), \quad (3.10)$$

$$C_{\mu\nu}^\gamma = \sum_j \gamma_{ij} C_{\mu\nu}(j, i)_{E.T.}, \quad (3.11)$$

$$C_{\mu\nu}^\alpha = \sum_j \alpha_{ij} C_{\mu\nu}(j, i)_{E.T.} \quad (3.12)$$

with

$$\alpha_{ij} = \frac{a^2}{(2\pi)^2} \int_{\Omega_B} d^2\mathbf{k} e^{i\mathbf{k}\cdot(\mathbf{R}_i - \mathbf{R}_j)} \alpha(\mathbf{k}). \quad (3.13)$$

The parameters not directly connected to the Green's function are μ , d_s , f , χ_s , defined in Appendix. In principle there are different ways to calculate these parameters: decoupling approximation, projection on the basis, use of linearized equations of motion. However, as discussed in Refs. [15,27], there is only one definite way to fix them: in order to have the right representation the Green's function must satisfy the equation

$$\lim_{j \rightarrow i^-} S(i, j) = \langle \Psi(i) \Psi^\dagger(i) \rangle, \quad (3.14)$$

where the r.h.s. is calculated by means of the Pauli principle.

Use of this equation leads to the following self-consistent equations

$$C_{23} = 0, \quad (3.15)$$

$$C_{24} = 3C_{12}^\gamma - \frac{3C_{12}^\gamma C_{22}}{I_{22}}, \quad (3.16)$$

$$C_{34} = -\frac{3C_{13}^\gamma C_{33}}{I_{33}}, \quad (3.17)$$

$$n_T = 4 - 2(C_{11} + C_{22} + C_{33}), \quad (3.18)$$

where $n_T = n_p + n_d$ is the total particle number and n_p is the number of p electrons. Equations (3.4)-(3.9) and (3.15)-(3.18) constitute a set of coupled equations which will fix the parameters in a self-consistent way.

Summarizing, we have ten parameters and ten self-consistency equations which allow us to compute the Green's function and the properties of the system in a fully self-consistent way.

Results of calculations are presented in the next Section. As as a comparison we also present results in the case where we do not take into account the Pauli principle and we express the parameters d_s , f , χ_s by means of the following decoupling equations

$$f \approx -C_{11}^{\gamma\gamma} [C_{12}^{\gamma} + C_{13}^{\gamma}], \quad (3.19)$$

$$d_s \approx [C_{12}^{\gamma\alpha} + C_{13}^{\gamma\alpha}] [C_{22}^{\alpha} + 2C_{23}^{\alpha} + C_{33}^{\alpha}], \quad (3.20)$$

$$\chi_s \approx -2 [C_{22}^{\alpha} + 2C_{23}^{\alpha} + C_{33}^{\alpha}]^2. \quad (3.21)$$

It should be noted that for certain values of the external parameters some instabilities appear in the iteration procedure and no solution of the self-consistent equations is found. This aspect is not present when the decoupling scheme (3.19)-(3.21) is used and may be related to the fact that more asymptotic fields are necessary in order to have a proper representation for the Green's function [27].

IV. RESULTS

This Section is organized as follows. The first part is devoted to compare the results of our calculations with the data of numerical analysis by Quantum Monte Carlo and exact diagonalization. As it will be shown in Sec. IV A, for all local quantities the agreement between numerical and COM results is excellent. Once we are confident to have a reasonable solution of the model, we go to the next step where we study some physical properties in order to verify if the p-d model is a realistic model for cuprate superconductors. This is done in the second part, Sections IV B and IV C, where the density of states and Fermi surface are analyzed. In this study the values of the model parameters have been taken according to the results suggested by *ab initio* calculation [28]: $t = 1eV$, $U = 6eV$, $\Delta = 2eV$, where $\Delta = \varepsilon_d + U - \varepsilon_p$ is the charge-transfer energy.

In this work all energy are given in units of t and measured with respect to the atomic level $\varepsilon_p = 0$.

A. Comparison with QMC data

Here we compare COM results with QMC calculations and Lanczos diagonalization results [29], [30], [31].

We introduce the squared local magnetic moment for d electrons as

$$S_z^2 = \frac{1}{N} \sum_i \langle [n_{d\uparrow}(i) - n_{d\downarrow}(i)]^2 \rangle. \quad (4.1)$$

This quantity can be expressed for paramagnetic case through the double occupancy and the number of d electrons as follows: $S_z^2 = n_d - 2D$.

Following Ref. [29] we can distinguish two different regimes according to the values of the U Hubbard repulsion and the charge-transfer energy Δ . In the region $U > \Delta$ the insulating properties of the system are characterized by a charge-transfer gap. Instead, in the region

$U < \Delta$ the system is in a Mott-Hubbard regime. Both regions are studied in the following.

In Fig. 1 and Fig. 2 we plot the squared local magnetic moment against the parameters Δ and U , respectively. S_z^2 is an increasing function of these parameters. Figure 1 shows that the local magnetic moment S_z^2 takes the smallest value when Δ approaches zero; in such case p and d upper Hubbard levels coincide and due to strong mixing the double occupancy takes a large value.

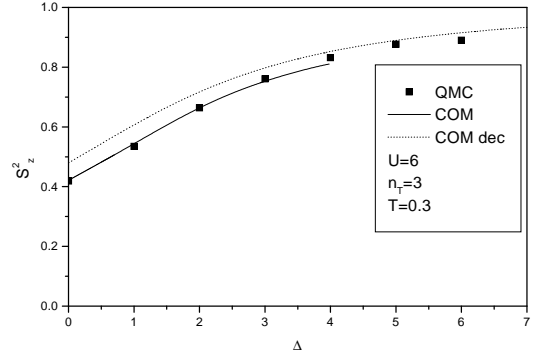


FIG. 1. The squared local magnetic moment S_z^2 against the parameter Δ ; the values of external parameters U , n_T and T are given in the figure. The solid line is COM prediction with Pauli principle, the dotted one with decoupling. The squares are QMC data [29].

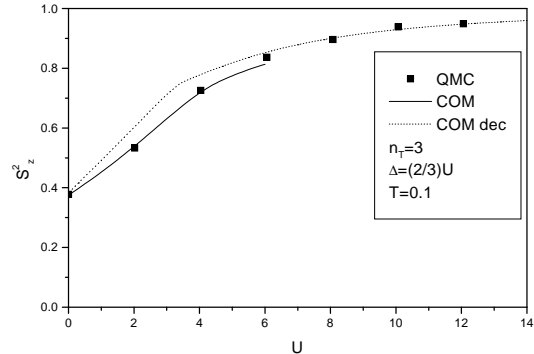


FIG. 2. The squared local magnetic moment S_z^2 against the parameter U ; the values of external parameters n_T , Δ and T are given in the figure. The solid line is COM prediction with Pauli principle, the dotted one with decoupling. The squares are QMC data [29].

Instead, when Δ becomes larger than U the system changes from charge-transfer insulator to Mott-Hubbard insulator and the local magnetic moment S_z^2 becomes independent on Δ . In this regime we are addressing a single-band 2D Hubbard model solution.

An increasing behaviour of S_z^2 is also possible for charge-transfer insulator as it is shown in Fig. 2, where

Δ is taken equal to $2U/3$. In such case double occupancy of d electrons decreases with increasing distance between bands and the local magnetic moment saturates.

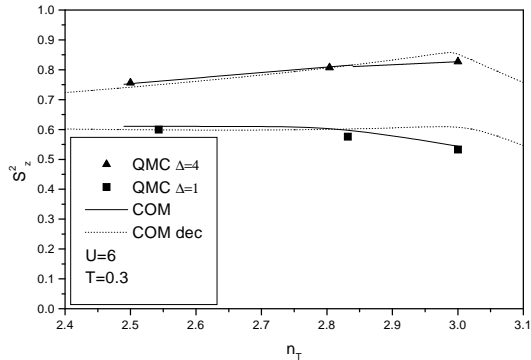


FIG. 3. The squared local magnetic moment S_z^2 against n_T for $\Delta = 1$ and $\Delta = 4$; the values of external parameters U and T are given in the figure. The solid line is COM prediction with Pauli principle, the dotted one with decoupling. The squares and the triangles are QMC data [29].

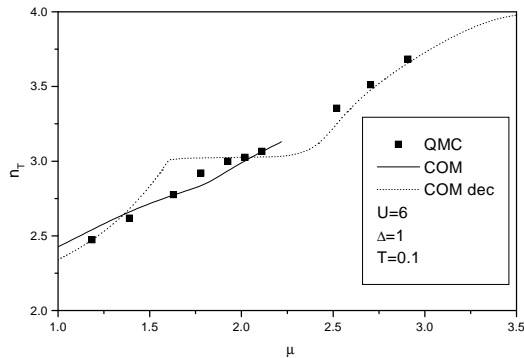


FIG. 4. The n_T - μ plot for the values of external parameters $U = 6$, $\Delta = 1$ and $T = 0.1$. The squares are QMC data [29], the solid line is COM prediction with Pauli principle, the dotted one is with decoupling.

The dependence of the squared local magnetic moment on the total number of particles n_T for $\Delta = 1$ and $\Delta = 4$ and for the values of external parameters $U = 6$, $T = 0.3$ is shown in Fig. 3.

We also report results for the case when the parameters d_s, f, χ_s are expressed by means of decoupling equations (3.19)-(3.21) (dotted line).

In all cases the agreement with QMC results is very good, specially in the case when we take into account the Pauli principle.

From Fig. 3 we see that the local magnetic moment only slightly changes with doping. Such fact was also observed in neutron scattering experiments on

$La_{2-x}Sr_xCuO_4$ [32], where it was stated that doping destroys antiferromagnetic spin correlations but does not destroy local magnetic moments.

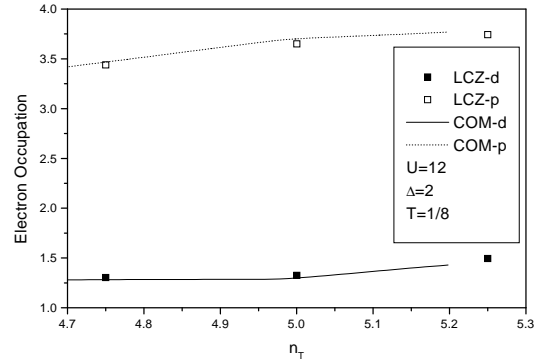


FIG. 5. n_d and n_p against the total electron occupation $n_T = n_d + 2n_p$ for the values of external parameters $U = 12$, $\Delta = 2$ and $T = 1/8$. The squares are Lanczos diagonalization results [30], the solid and dotted lines are COM calculation.

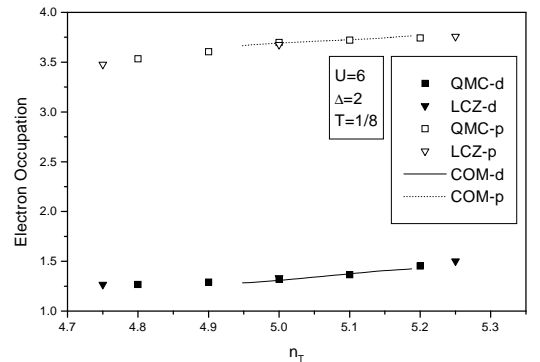


FIG. 6. n_d and n_p against the total electron occupation $n_T = n_d + 2n_p$ for the values of external parameters $U = 6$, $\Delta = 2$ and $T = 1/8$. The squares and the triangles are QMC and Lanczos diagonalization results, respectively [30]; the solid and dotted lines are COM predictions.

In a previous paper [22] the transition between p level and the lower Hubbard level ξ was not taken into account, and the the number of d electrons n_d was calculated only approximately. As a result the agreement with QMC data was only qualitative.

In Fig. 4 the dependence of n_T on the chemical potential is drawn for $U = 6$, $\Delta = 1$ and $T = 0.1$; a good agreement between COM predictions and QMC results is found. As a comparison, it is also reported the case when the Pauli principle is not taken into account; in this case the agreement with QMC simulations is not so good.

In Fig. 5 and Fig. 6 we present also a very good agreement of our results with Lanczos diagonalization and QMC calculations given in Ref. [30]. The authors of this

work write the full number of holes as $n = n_{Cu} + 2n_O$, where the double number of oxygen holes is due to the two oxygen ions in the cell. We remind that in the p-d model there are two bonding and two nonbonding electrons per site. To make a comparison with results of Ref. [30] we have to take into account the Fermi occupation number of these two unbonding orbitals and to rewrite equation (3.18) as

$$n_T = 4 - 2(C_{11} + C_{22} + C_{33}) + \frac{2}{\exp((\varepsilon_p - \mu)/T) + 1}. \quad (4.2)$$

For the values of external parameters given in Fig. 5 and Fig. 6 the system is in the charge-transfer regime and in the vicinity of $n_T = 1$ holes prefer to go to p orbitals and electrons to d orbitals.

In Fig. 7 it is shown the dependence of the charge-transfer susceptibility at $\mathbf{q} = 0$ on charge-transfer energy Δ . This quantity [30] is given by

$$\lim_{\mathbf{q} \rightarrow 0} \chi_{CT}(\mathbf{q}) = \frac{\partial}{\partial \Delta} \langle n_d - 2n_p \rangle. \quad (4.3)$$

The agreement between COM predictions and QMC simulations is very good.

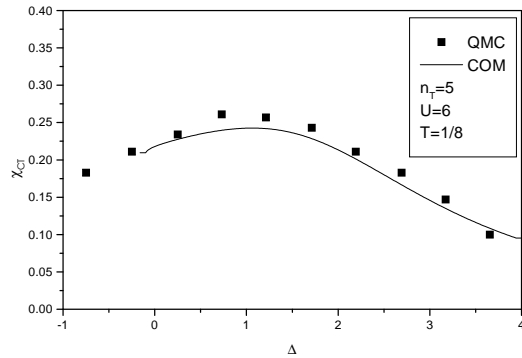


FIG. 7. The charge-transfer susceptibility χ_{CT} at $\mathbf{q} = 0$ versus Δ for the values of external parameters $U = 6$, $n_T = 5$ and $T = 1/8$; the squares are QMC results [30] and the solid line is COM prediction.

In Fig. 8, Fig. 9 and Fig. 10 we plot the quantities n_d , S_z^2 and D against the charge-transfer gap Δ for the values of external parameters $U = 6$, $n_T = 5$ and $T = 1/8$. The agreement between COM prediction and QMC simulation [30] is excellent. The dependence of the calculated quantities on external parameters has the same behaviour as in Fig. 1. We want to note once more that the holes introduced in CuO_2 planes reside primarily on oxygen sites, as it is well-known experimentally.

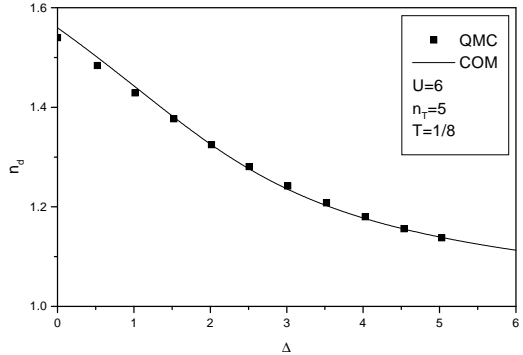


FIG. 8. The n_d - Δ plot for the values of external parameters $U = 6$, $n_T = 5$ and $T = 1/8$; the squares are QMC results [30] and the solid line is COM prediction.

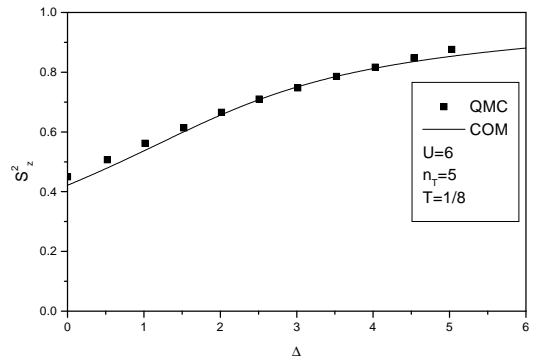


FIG. 9. The squared magnetic moment S_z^2 against Δ for the values of external parameters $U = 6$, $n_T = 5$ and $T = 1/8$; the squares are QMC results [30] and the solid line is COM result.

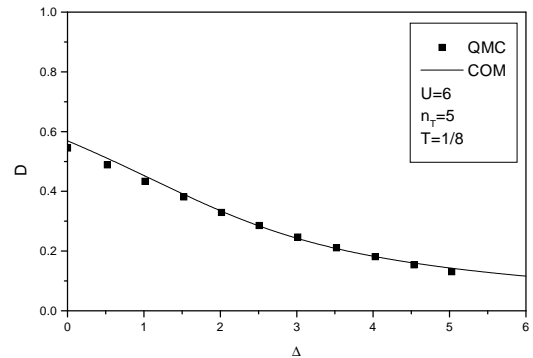


FIG. 10. The double occupancy D versus Δ for the values of external parameters $U = 6$, $n_T = 5$ and $T = 1/8$; the squares are QMC results [30] and the solid line is COM prediction.

In Fig. 11 and Fig. 12 the band dispersion of Zhang-Rice singlet for $n_T = 2.5$ and $n_T = 2.75$ is shown. The squares are QMC data from [31] and the solid line is the COM result. The data differ significantly only for the values of dispersion energies far from the chemical potential.

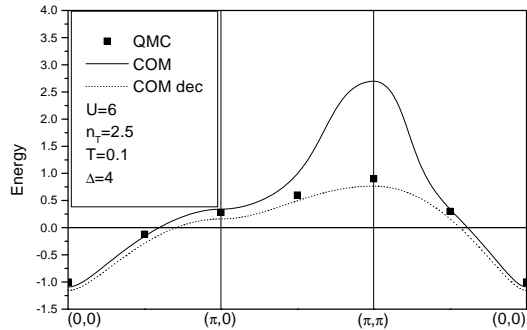


FIG. 11. The band structure for the Zhang-Rice singlet for $n_T = 2.5$. The squares are QMC data [31], the solid line is COM prediction with Pauli principle, the dotted one is with decoupling.

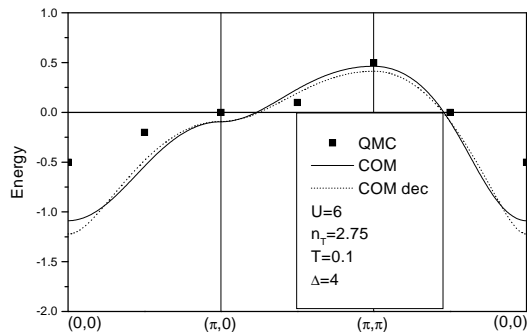


FIG. 12. The band structure for the Zhang-Rice singlet for $n_T = 2.75$. The squares are QMC data [31], the solid line is COM prediction with Pauli principle, the dotted one is with decoupling.

Summarizing, in this section we have presented a detailed comparison of COM results with the available data by numerical simulation. It is worth noticing that the formulation is fully self-consistent and no adjustable parameter is used.

B. Density of states

In this paragraph and in the next one we present an analysis of the band structures of the model and we give a description of the relevant physics near the Fermi level.

The density of states (DOS) for p and d electrons is respectively given by the following expressions

$$N_p(\omega) = \frac{a^2}{(2\pi)^2} \int_{\Omega_B} d^2\mathbf{k} \sum_{n=1}^4 \sigma_{11}^{(n)}(\mathbf{k}) \delta(\omega - E_n(\mathbf{k})), \quad (4.4)$$

$$N_d(\omega) = \frac{a^2}{(2\pi)^2} \int_{\Omega_B} d^2\mathbf{k} \sum_{n=1}^4 [\sigma_{22}^{(n)}(\mathbf{k}) + 2\sigma_{33}^{(n)}(\mathbf{k}) + \sigma_{33}^{(n)}(\mathbf{k})] \delta(\omega - E_n(\mathbf{k})), \quad (4.5)$$

where the spectral functions $\sigma_{\alpha\beta}^{(n)}(\mathbf{k})$ and the energy bands $E_n(\mathbf{k})$ can be calculated as indicated in Sec. II.

In Figs. 13, 14 and 15 we present the DOS of d electrons (solid line) and p electrons (dotted lines) for $U = 6$, $\Delta = 2$, $T = 0.001$ and for $n_T = 2.70$, 2.85 and 2.90, respectively. The solid vertical line at $\omega = 0$ indicates the chemical potential.

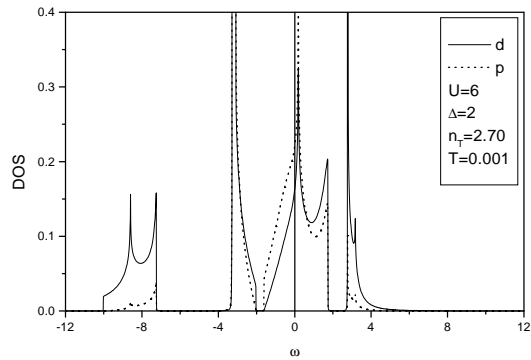


FIG. 13. p -DOS (dotted line) and d -DOS (solid line) for $n_T = 2.70$. With respect to the chemical potential $\varepsilon_p = -1.613$.

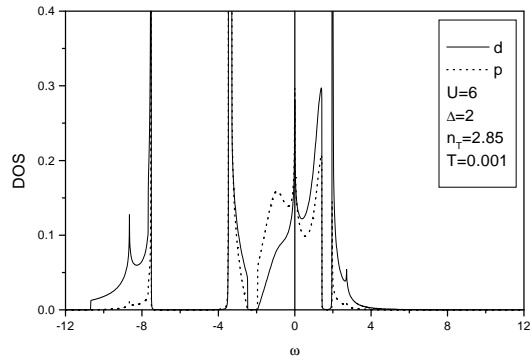


FIG. 14. p -DOS (dotted line) and d -DOS (solid line) for $n_T = 2.85$. With respect to the chemical potential $\varepsilon_p = -1.945$.

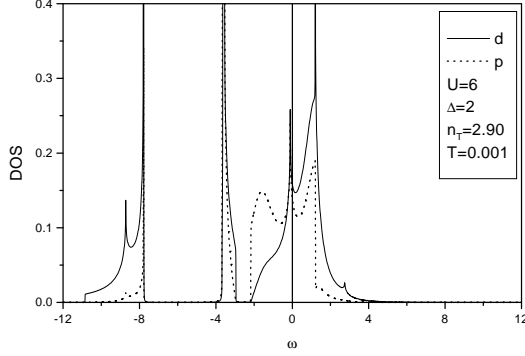


FIG. 15. p -DOS (dotted line) and d -DOS (solid line) for $n_T = 2.90$. With respect to the chemical potential $\varepsilon_p = -2.174$.

As it can be seen from these pictures there are four bands. The lower Hubbard band located at $\omega \approx -9$ represents the ξ excitations; this band is filled mainly by d electrons and it has a small fraction of p electrons. The upper Hubbard band, located at $\omega \approx 3$, comes from η operator excitations; it has mainly the weight of d electrons. The band coming from the ε_p atomic level is located around $\omega \approx -3$. It is filled by p electrons, but due to strong mixing it also contains a large fraction of d electrons. Finally, the Zhang-Rice singlet band is situated around the chemical potential; this band has almost equal fraction of p and d electrons.

We want to stress the importance of studying the Zhang-Rice excitation as independent field in the initial set (2.5). As shown in Ref. [24], if one does not initially consider the p_s excitation, the information about p and d electrons coupling is lost after taking averages (2.20), (2.21) and one does not get the band dispersion situated at the chemical potential when the total number of particles is $n_T \approx 3$.

The singlet coupling of p and d electrons was investigated by means of COM in the earlier work of Matsumoto *et al.* together with one of us [13]. They obtained the singlet excitation band at the chemical potential and studied how the density of states depends on the variation of the correlators.

In this work we considered the full p-d model, as described by Eq. (2.1), and we used additional equations supplied by Pauli principle (Eqs. (3.15) -(3.17)) to calculate the values of these correlators.

C. An analysis of the experimental data

We investigated the region of total number of electrons around $n_T = 3$, which corresponds to the initial situation where only one electron is in the copper d orbital due to the strong Hubbard repulsion and two electrons in the bounded p orbitals of oxygen.

In Fig. 16 the band structure for the Zhang-Rice singlet is drawn for the values of external parameters given in the pictures; we see that at the momentum $\mathbf{k} = (\pi, 0)$ such band has a saddle-point. This saddle-point leads to the van-Hove singularity in the density of states (see Fig. 13, Fig. 14 and Fig. 15) and it was observed in experiments [8–10].

We note that for $U = 6$ and $\Delta = 2$ the coincidence of the chemical potential and van-Hove singularity takes place at the value of total number of particles $n_T = 2.85$, corresponding to the hole doping $\delta = 0.15$. This results to an enhancement of the thermodynamical properties such as specific heat and spin magnetic susceptibility, as observed in the two-dimensional Hubbard model [13,14,33]. Upon increasing the particle number up to $n_T = 2.9$ the gap between the upper Hubbard band and the Zhang-Rice singlet band disappears.

In Fig. 17 and Fig. 18 we plot the Fermi Surface for the values of the external parameters $U = 6$, $\Delta = 2$ and $T = 0.001$ and for total number of particles $n_T = 2.7$ and $n_T = 2.9$ respectively. The values of the temperature and of the total number of particles were chosen in order to compare the Fermi surface calculated by means of COM with the experimental one measured by Ino *et al* [34] and shown by the circles in the pictures.

We see that at the total number of particles $n_T = 2.85$, when the chemical potential crosses the van Hove singularity, the Fermi surface changes its shape from the electron-like in the overdoped regime ($n_T = 2.7$) to the hole-like in the underdoped regime ($n_T = 2.9$). This is in agreement with ARPES results [34] and Hall coefficient measurements [35].

As a comparison, we also plot the Fermi Surface when we do not take into account the Pauli principle (dotted line); the agreement with experimental results is not good in this case.

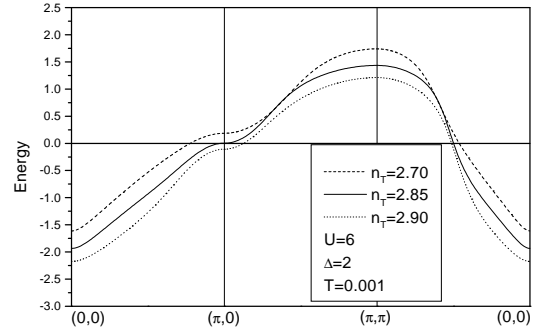


FIG. 16. The band structure for the Zhang-Rice singlet for $n_T = 2.70, 2.85, 2.90$ and for $U = 6$, $\Delta = 2$ and $T = 0.001$.

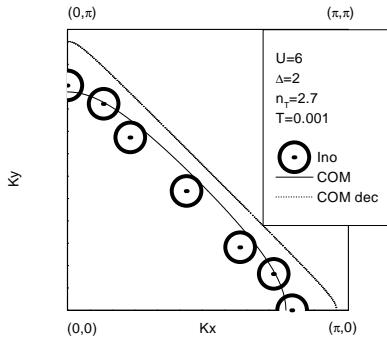


FIG. 17. The Fermi Surface for $U = 6$, $\Delta = 2$, $n_T = 2.7$ and $T = 0.001$; the solid line is COM prediction with Pauli principle, the dotted one with decoupling. The circles are experimental results [34].

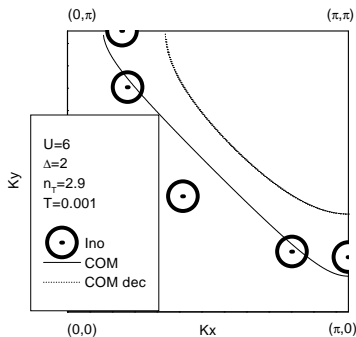


FIG. 18. The Fermi Surface for $U = 6$, $\Delta = 2$, $n_T = 2.9$ and $T = 0.001$; the solid line is COM prediction with Pauli principle, the dotted one with decoupling. The circles are experimental results [34].

V. CONCLUSIONS

The p-d model was studied in order to describe energetic properties of charge excitations in the CuO_2 planes of cuprates in the normal state. Excitations are described in terms of composite operators in the CuO_2 cluster. The most important excitation appears to be the Zhang-Rice singlet. The oxygen hole doped into the CuO_2 plane couples with Cu electron forming a singlet state. The band of these states is located between the oxygen level and the copper upper Hubbard atomic level. By hole doping the Fermi level crosses this band and at definite value of doping it coincides with a van-Hove singularity in the density of states. This singularity is formed by the saddle shape of the band dispersion at the Brillouin zone points $(\pi, 0)$ and $(0, \pi)$ as it was also obtained in experiments and in QMC calculations.

The large volume of the Fermi surface at low doping results from the small spectral weight of the field describing p electrons dressed by spin-flips of d electrons. Such reduction of the spectral weight is possible due to

its redistribution to the other bands strongly mixed with Zhang-Rice singlet band.

By using a four-pole approximation in the framework of the Composite Operator Method various local quantities have been calculated as functions of model and physical parameters. The results of calculations have been presented in Sec. IV A and compared with the results of numerical analysis.

We want to stress the relevance of Pauli principle in treating with strongly correlated electronic systems within our method. The comparison of COM results with numerical data, concerning local properties and band structures, and experimental measurements obtained by Ino *et al* [34] looks to have a good agreement when we take into account the Pauli principle in computing the fermionic propagator.

As last remark, we want to note that we can calculate the two-particle Green's functions in the one-loop approximation [13] by using the single-particle propagator. Calculations in this direction are now in progress.

ACKNOWLEDGMENTS

We wish to thank Dr. A. Avella for fruitful discussions and useful comments.

APPENDIX: THE MATRICES I AND M AND THE SELF-CONSISTENCY PARAMETERS.

In this appendix we give the explicit form of matrices I and m and we also report the expression of the self-consistency parameters.

The I matrix is diagonal and its elements are:

$$I_{11} = 1, \quad I_{22} = 1 - n_d/2, \quad I_{33} = n_d/2, \quad (\text{A1})$$

$$I_{44} = 3(n_d - 2D - \alpha(\mathbf{k})\chi_s) + 4a_s - 9\left(\frac{c^2}{I_{22}} + \frac{b^2}{I_{33}}\right). \quad (\text{A2})$$

The quantities n_d and D are the particle number and the double occupancy per site of d electrons, respectively:

$$n_d = \langle d^\dagger(i) d(i) \rangle, \quad (\text{A3})$$

$$D = \langle n_\uparrow(i) n_\downarrow(i) \rangle. \quad (\text{A4})$$

The other parameters are defined by

$$b = \langle p^\gamma(i) \eta^\dagger(i) \rangle, \quad c = \langle p^\gamma(i) \xi^\dagger(i) \rangle, \quad (\text{A5})$$

$$a_s = \langle p^\gamma(i) p_s^\dagger(i) \rangle, \quad \chi_s = \frac{1}{3} \langle n_k(i) n_k^\alpha(i) \rangle. \quad (\text{A6})$$

The m matrix is hermitician and its elements have the expressions:

$$\begin{aligned}
m_{11} &= \varepsilon_p - \mu, & m_{12} &= 2tI_{22}\gamma(\mathbf{k}), \\
m_{13} &= 2tI_{33}\gamma(\mathbf{k}), & m_{14} &= 0, \\
m_{22} &= (\varepsilon_d - \mu)I_{22} + 2t(c - b), & m_{23} &= 2(b - c), \\
m_{24} &= 2tI_{\pi p_s}, & m_{34} &= -m_{24},
\end{aligned} \tag{A7}$$

$$\begin{aligned}
m_{33} &= (\varepsilon_d + U - \mu)I_{33} - 2t(b - c), \\
m_{44} &= (\varepsilon_p - \mu)I_{44} + 2tI_{\kappa_s p_s} + t_p I_{\pi p_s},
\end{aligned} \tag{A8}$$

where

$$I_{\pi p_s} = \frac{3}{2}(n_d - 2D - \alpha(\mathbf{k})\chi_s) + 2a_s - \frac{t_p(b - c)}{2t}, \tag{A9}$$

$$I_{\kappa_s \xi} = \frac{1}{2t}(2tI_{\pi p_s} - \varepsilon_{p\xi}I_{22} - t_p(c - b)), \tag{A10}$$

$$I_{\kappa_s \eta} = -\frac{1}{2t}(2tI_{\pi p_s} + \varepsilon_{p\eta}I_{33} + t_p(b - c)), \tag{A11}$$

$$\begin{aligned}
I_{\kappa_s p_s} &= 6(-b - f + d_s\alpha(\mathbf{k})) - 4b_s \\
&\quad - 3\left(c\frac{I_{\kappa_s \xi}}{I_{22}} + b\frac{I_{\kappa_s \eta}}{I_{33}}\right).
\end{aligned} \tag{A12}$$

The parameters b_s , f , and d_s are defined by

$$b_s = \langle d^\alpha(i)p_s^\dagger(i) \rangle, \tag{A13}$$

$$f = \langle p^\gamma(i)d^\dagger(i)p^\gamma(i)p^{\gamma\dagger}(i) \rangle, \tag{A14}$$

$$d_s = \frac{1}{3}\langle n_k^\alpha(i)\sigma_k p^\gamma(i)d^\dagger(i) \rangle. \tag{A15}$$

-
- * Institute of Materials Science and Applied Research, Sauletekio al. 9 - III, 2040 Vilnius, Lithuania
- [1] The Theory of Superconductivity in the High-Tc Cuprates by P. W. Anderson, Princeton Series in Physics (1997).
- [2] High-Temperature Superconductivity: Experiment and Theory by N.M. Plakida, Berlin Springer (1995).
- [3] P. W. Anderson, Science, **235**, 1196 (1987); Anderson, P. W., G. Baskaran, Z. Zou, and T. Hsu, Phys. Rev. Lett. **58**, 2790 (1987).
- [4] F.C. Zhang and T.M. Rice, Phys. Rev. B **38**, 3759 (1988).
- [5] V. Emery and G. Reiter, Phys. Rev. B **38**, 4547 (1988).
- [6] A.F. Barabanov, V.M. Beresovsky, L.A. Maksimov and E. Zasinias, JETP, **83**, 819 (1996).
- [7] A.F. Barabanov, L.A. Maksimov, O.V. Urazaev and E. Zasinias, JETP letters, **66**, 182, (1997).
- [8] J.G. Tobin *et al*, Phys. Rev. B **45**, 5563 (1992); R. Manzke *et al*, Surface Sci. **269**, 1066 (1992).
- [9] A.A. Abrikosov, J.C. Campuzano and K. Gofron, Physica C, **214**, 73 (1993).

- [10] K. Gofron *et al*, Phys. Rev. Lett. **73**, 3302 (1994).
- [11] B.O. Wells *et al*, Phys. Rev. Lett. **74**, 964 (1995).
- [12] S. Ishihara, H. Matsumoto, S. Odashima, M. Tachiki and F. Mancini, Phys. Rev. B **49**, 1350 (1994).
- [13] F. Mancini, S. Marra and H. Matsumoto, Physica C **244**, 49 (1995); **250**, 184 (1995); **252**, 361 (1995).
- [14] F. Mancini, H. Matsumoto and D. Villani, Phys. Rev. B **57**, 6145 (1998).
- [15] A. Avella, F. Mancini, D. Villani, L. Siurakshina, V. Yu. Yushankhai, Int. Journ. Mod. Phys. B **12**, 81 (1998).
- [16] F. Mancini and A. Avella, Condensed Matter Physics, **1**, 11 (1998).
- [17] K.W. Becker, W. Brenig and P. Fulde, Z. Phys. B **81**, 165 (1990); H. Mori, Progr. Theor. Phys. **33**, 423 (1965); *ibid* **34**, 399 (1965); A.J. Fedro, Yu Zhou, T.C. Leung, B.N. Harmon and S.K. Sinha, Phys. Rev. B **46**, 14785 (1992); P. Fulde, Electron Correlations in Molecules and Solids (Springer-Verlag, Berlin-Heidelberg, 1993); N.M. Plakida, V.Yu. Yushankhai and I.V. Stasyuk, Physica C **162-164**, 787 (1989); B. Mehlig, H. Eskes, R. Hayn and M.B.J. Meinders, Phys. Rev. B **52**, 2463 (1995).
- [18] D.J. Rowe, Rev. Mod. Phys. **40**, 153 (1968); L.M. Roth, Phys. Rev. **184**, 451 (1969); J. Beenen and D.M. Edwards, Phys. Rev. B **52**, 13636 (1995).
- [19] O.K. Kalashnikov and E.S. Fradkin, Phys. Stat. Sol. (b) **59**, 9 (1973); W. Nolting, Z. Phys. B **255**, 25 (1972); G. Geipel and W. Nolting, Phys. Rev. B **38**, 2608 (1988); W. Nolting and W. Borgel, Phys. Rev. B **39**, 6962 (1989); A. Lonke, J. Math. Phys. **12**, 2422 (1971).
- [20] H. Matsumoto and F. Mancini, Phys. Rev. B **55**, 2095 (1997).
- [21] H. Matsumoto, T. Saikawa and F. Mancini, Phys. Rev. B **54**, 14445 (1996).
- [22] F. Mancini, S. Marra, D. Villani and H. Matsumoto, Physics Letters A **210**, 429 (1996).
- [23] F. Mancini, S. Marra, and D. Villani, Condensed Matter Physics **7**, 133 (1996).
- [24] V. Fiorentino, F. Mancini, A.F. Barabanov, Physica B **284**, 1195 (2000).
- [25] For a review see E. Dagotto, Rev. of Mod. Phys. **66**, 763 (1994).
- [26] H. Matsumoto and M. Tachiki, Progr. Theor. Phys. Supplement **101**, 353 (1990).
- [27] F. Mancini and A. Avella, cond-mat/0006377.
- [28] E. B. Stechel and D. R. Jennison, Phys. Rev. B, **38**, 4632 (1988); A. K. McMahan, R. M. Martin and S. Satpathy, Phys. Rev. B, **38**, 6650 (1989); M. S. Hybertsen, M. Schluter and N. E. Christensen, Phys. Rev. B, **39**, 9028 (1989); J. B. Grant and A. K. McMahan, Phys. Rev. B, **46**, 8440 (1992).
- [29] G. Dopf, A. Muramatsu and W. Hanke, Phys. Rev. B **41**, 9264 (1990).
- [30] R.T. Scalettar, D.J. Scalapino, R.L. Sugar and S.R. White, Phys. Rev. B **44**, 770 (1991).
- [31] G. Dopf, J. Wagner, P. Dieterich, A. Muramatsu and W. Hanke, Phys. Rev. Lett. **68**, 2082 (1992).
- [32] R.J. Birgeneau *et al.*, Phys. Rev. B **38**, 6614 (1988).
- [33] F. Mancini, H. Matsumoto and D. Villani, Journ. of Physical Studies **3**, 474 (2000).
- [34] A. Ino, C. Kim, T. Mizokawa, Z.-X. Shen, A. Fujimori, M. Takaba, K. Tamasaku, H. Eisaki, S. Uchida, J. Phys. Soc. Jpn. **68**, 1496 (1999).
- [35] T. Plackowski and M. Matusiak, Phys. Rev. B **60**, 14872 (1999).